

Communication

Energy Backflow in Tightly Focused Fractional Order Vector Vortex Beams with Binary Topological Charges

Yan Wu, Xiaobo Hu , Yuhua Li * and Ruipin Chen * 

Key Laboratory of Optical Field Manipulation of Zhejiang Province, Department of Physics, Zhejiang Sci-Tech University, Hangzhou 310018, China; phys_wy@zstu.edu.cn (Y.W.)

* Correspondence: yuhuali@zstu.edu.cn (Y.L.); chenrp@zstu.edu.cn (R.C.)

Abstract: Using the Richards–Wolf diffraction integral, the longitudinal energy evolution on the focal plane of the fractional order vector vortex (FOVV) beams was studied. These beams possessed a vortex topological charge n and a polarization topological charge m , and were subjected to tight focusing through a larger numerical aperture. Our investigation revealed the existence of backflow energy when the binary topological charges n and m satisfied the conditions of $n + m = 2$ or $n - m = -2$. The component circularly polarized vortex beams of $e^{-i2\phi}\hat{e}_+$ (i.e., the minus second-order vortex right circularly polarized beam) and $e^{i2\phi}\hat{e}_-$ (i.e., the second-order vortex left circularly polarized beam) played significant roles in the generation of reverse energy flux at the focal region. For FOVV beams with binary topological charges n and m , whose sum and difference were integers, the longitudinal energy on the focal plane exhibited axial symmetry. If the sum or the difference of the topological charges n and m was not an integer, the axisymmetric longitudinal energy on the focal plane was disrupted.

Keywords: fractional-order vector vortex; energy backflow; reverse energy flux; poynting vector



Citation: Wu, Y.; Hu, X.; Li, Y.; Chen, R. Energy Backflow in Tightly Focused Fractional Order Vector Vortex Beams with Binary Topological Charges. *Photonics* **2023**, *10*, 820. <https://doi.org/10.3390/photonics10070820>

Received: 19 June 2023
Revised: 10 July 2023
Accepted: 12 July 2023
Published: 14 July 2023



Copyright: © 2023 by the authors. Licensee MDPI, Basel, Switzerland. This article is an open access article distributed under the terms and conditions of the Creative Commons Attribution (CC BY) license (<https://creativecommons.org/licenses/by/4.0/>).

1. Introduction

When vector vortex beams with inhomogeneous polarized fields are tightly focused by a high numerical aperture (NA) lens, the state of polarization (SOP) and the phase can be rearranged. In particular, the strong longitudinal field was initially discovered by Youngworth and Brown [1], when a radially polarized beam passed through a high NA. In 2007, A. V. Novitsky and D. V. Novitsky demonstrated the negative propagation of vector beams by superimposing TE- and TM-polarized electromagnetic Bessel beams [2]. Then, the properties of a tightly focused circularly polarized optical vortex with topological charges of 2 and 3 were investigated in Ref. [3]. In the meantime, using theoretical analysis and numerical simulation, Khonina et. al. found that when the second-order radial polarized vector beam was tightly focused, the negative energy flux density was maximum [4]. Subsequently, Kotlyar et. al. found that if a non-zero E-field intensity was found in the focus of a circularly polarized optical vortex with phase singularity or a higher-order azimuthally polarized beam with polarization singularity, the energy backflow would occur at the center of the focal plane [5]. Then, further investigation of vector vortex fields passing through a high NA yielded valuable results, enabling the control of the negative energy flow [6–8].

Energy backflow was observed experimentally within super oscillatory optical fields [9]. Kotlyar and Nalimov found that a strongly focused, linearly polarized optical vortex with a topological charge of 2 not only exhibited a reverse energy flow, but also induced the right-handed circular polarization of light in the near-focus region [10], which led to the spin-orbital angular momentum conversion. These significant findings open up the probability of capturing and manipulating an absorbing spherical microparticle positioned at the optical axis within the focal region. Focusing the vector vortex beams is a widely used

technique in optical data storage [11,12], optical communication [13–16], detection and imaging [17,18], and optical micromanipulation [19]. Because the focusing characteristics rely closely on the polarization of the light, the vector and the vortex natures of the focused beam are of vital importance. By utilizing a spatial light modulator (SLM) in conjunction with a common path interferometric arrangement, fractional vector vortex beams with arbitrary topological charges could be generated [20]. However, the characteristics of the longitudinal energy flow within tightly focused fractional order vector vortex (FOVV) beams remain unclear.

Using the Richards–Wolf diffraction integral [21], the focusing characteristics of the FOVV beams were examined. For those FOVV beams, the axisymmetric longitudinal backflow energy appeared within the focal region when the vortex topological charge n and the polarization topological charge m satisfied $n + m = 2$ or $n - m = -2$. Considering that the fractional vortices can be expressed as a superposition of the vortex circularly polarized beams, the contributions of the vortex circularly polarized laser fields to the negative energy flux within the focal region of a high NA were investigated. We found that the incident minus second-order vortex right circularly polarized beam described by $e^{-i2\phi}\hat{e}_+$ and the second-order vortex left circularly polarized beam described by $e^{i2\phi}\hat{e}_-$ played significant roles in the generation of reverse energy flow at the focal region. The case of the beam of $e^{i2\phi}\hat{e}_-$ agreed well with the research results in Ref. [3]. Moreover, the property of the longitudinal energy of the vortex right circularly polarized laser fields with integer vortex order were same as that of the vortex left circularly polarized laser fields with the corresponding opposite negative integer vortex order. The cases of the vortex left circularly polarized laser fields with integer vortex order and the vortex right circularly polarized laser fields with the corresponding opposite negative integer vortex order were identical, too. For FOVV beams with binary topological charges n and m , whose sum and the difference are integers, the longitudinal energy on the focal plane will exhibit axial symmetry. If the sum or the difference of the topological charges n and m is not an integer, the axisymmetric longitudinal energy on the focal plane will be disrupted.

2. Theory and Methods

According to the Richards–Wolf diffraction theory, the electric field of the laser beam at the position $q(r_q, \phi_q, z_q)$ near the focus of an aplanatic system could be obtained by the following diffraction integral formula [5,21]:

$$\begin{pmatrix} E_x \\ E_y \\ E_z \end{pmatrix} = -\frac{if}{\lambda} \int_0^{\theta_m} A(\theta) \sin \theta \sqrt{\cos \theta} \cdot \exp(ikz_q \cos \theta) \times \int_0^{2\pi} \exp(ikr_q \sin \theta \cos(\phi - \phi_q)) \times \begin{pmatrix} 1 + \cos^2 \phi (\cos \theta - 1) & \sin \phi \cdot \cos \phi (\cos \theta - 1) \\ \sin \phi \cdot \cos \phi (\cos \theta - 1) & 1 + \sin^2 \phi (\cos \theta - 1) \\ -\sin \theta \cos \phi & -\sin \theta \sin \phi \end{pmatrix} \begin{bmatrix} E_{in,x} \\ E_{in,y} \end{bmatrix} d\phi \cdot d\theta, \tag{1}$$

where $E_{in,x}$ and $E_{in,y}$ are the components of the transverse electric field in the incident pupil of the high-aperture system along the x and y axes, respectively. $A(\theta)$ denotes the amplitude of the incident electric field. θ and ϕ are the polar and azimuthal angles of the incident pupil's coordinates. θ_m is the angular semi-aperture. f is the focal length of the aperture, and λ is the wavelength of the laser.

The time-averaged energy flux density (Poynting vector) is $\vec{S} = c/(8\pi) \text{Re}(\vec{E} \times \vec{H}^*)$, where the magnetic field \vec{H} could be obtained by curling the electric field as $\vec{H} = \frac{-i}{k} \nabla \times \vec{E}$, and k is the wavenumber. The longitudinal component of the Poynting vector is $S_z = \text{Re}(E_x H_y^* - E_y H_x^*)$. The incident light beam with vortexes travels along the z axis, and the electric field is confined in the xoy plane, taking the form [22]:

$$\vec{E}_{in} = E_{in,x} \hat{e}_x + E_{in,y} \hat{e}_y = e^{in\phi} \left(\cos(m\phi) \hat{e}_x + \sin(m\phi) \hat{e}_y \right), \tag{2}$$

where n and m denote the vortex and the polarization topological charges, respectively, which provide binary vortices phases manipulation.

3. Results

The Richards–Wolf diffraction theory can be utilized to simulate the sharp focusing FOVV beams. The longitudinal energy flow and the intensities of the transvers electric fields of FOVV beams on the focal plane were investigated in detail. In our calculations, the incident light possessed a Gaussian intensity distribution with a wavelength of $\lambda = 532$ nm, and the NA = 0.98, corresponding to a focal length of $f = 8\lambda$.

The focusing fields on the focal plane of FOVV beams with $n = 1.5$ and $m = 0.2, 0.5,$ and $0.8,$ respectively, are shown in Figure 1. The first column displays the intensity of the transverse electric field, while the second and third columns depict the longitudinal energy flow. From Figure 1(c₃), we can observe that there was no negative energy flow for the case of $n = 1.5$ and $m = 0.8$. Additionally, the longitudinal energy distribution lost axial symmetry about the optical axis. For the FOVV beam with $n = 1.5$ and $m = 0.2$ in Figure 1(a_{1–a₃}), although the axial symmetry was disrupted, there was a presence of the negative energy flow around the optical axis on the focal plane. For the FOVV beams with topological charges of $n = 1.5$ and $m = 0.5$ in Figure 1(b_{1–b₃}), the axisymmetric negative energy flow appeared. Now, the question arises: Will axial symmetrical negative energy flows occur when the topological charges n and m are half integers?

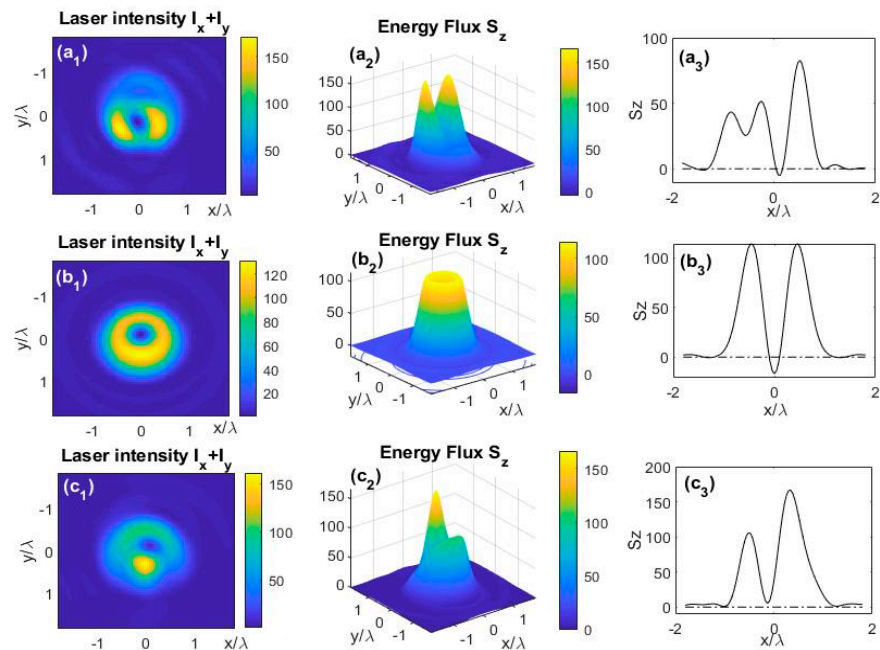


Figure 1. The intensity distributions of transverse light fields for tightly-focused beams at the focal plane, along with the corresponding longitudinal energy fluxes of vector vortex fields carrying fractional topological charges of (a_{1–a₃}) $n = 1.5, m = 0.2,$ (b_{1–b₃}) $n = 1.5, m = 0.5,$ and (c_{1–c₃}) $n = 1.5, m = 0.8.$

Figure 2 depicts the cases of FOVV beams with half-integer topological charges. It can be observed that for $n = 0.5, m = 1.5$ in Figure 2(a_{1–a₃}), and $n = 2.5, m = -0.5$ in Figure 2(b_{1–b₃}), axisymmetric backflow energy appears on the center of the focal plane. However, for $n = 2.5, m = 1.5$ in Figure 2(c_{1–c₃}), there was no backflow energy. Comparing the FOVV beams in Figure 2a,b, a common relationship existed in $n + m = 2$. When $n + m = 2$ was fulfilled, the distributions of the transverse light field intensity shown in Figure 2(a₁,b₁) were almost annular, with no transverse electric field in the center of the focal plane. For the cases of the FOVV beam with topological charges $n = 2.5$ and $m = 1.5,$ depicted in Figure 2(c_{1–c₃}), the annular structure of the transverse light field energy was

broken, with no backward energy on the focal plane, although the longitudinal energy flow was axisymmetric too.

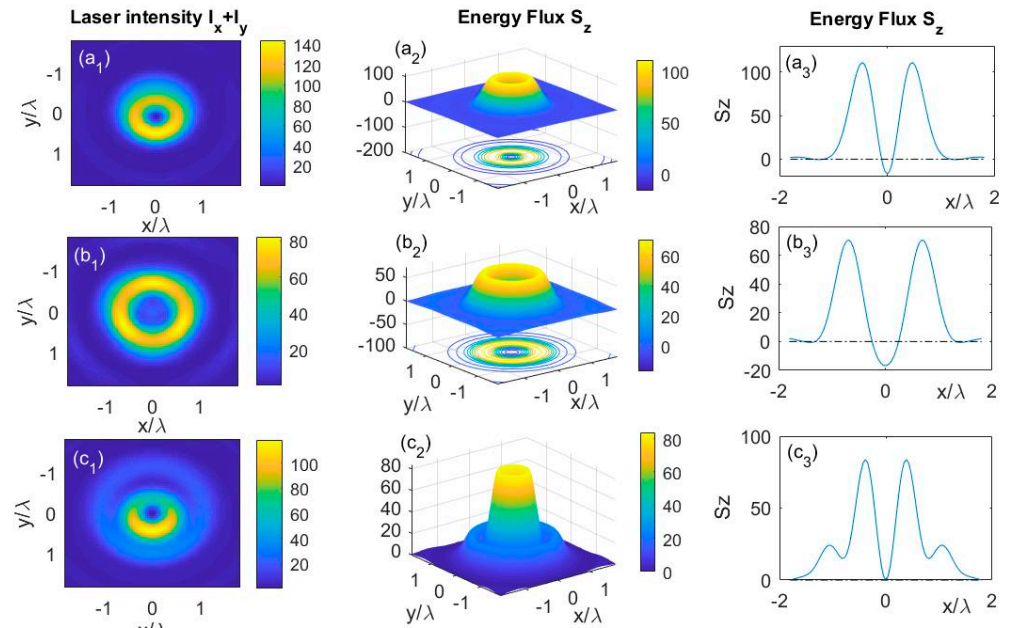


Figure 2. The intensity distributions of transverse light fields for tightly-focused beams at the focal plane, along with the corresponding longitudinal energy fluxes of vector vortex fields carrying fractional topological charges of (a₁–a₃) $n = 0.5, m = 1.5$, (b₁–b₃) $n = 2.5, m = -0.5$, and (c₁–c₃) $n = 2.5, m = 1.5$, respectively.

The focusing cases of the FOVV beams with non-half integer topological charges are shown in Figure 3. For $n = 1.6$ and $m = 3.1$ in Figure 3(c₁–c₃), there was almost no backflow energy, and the axial symmetry of the longitudinal energy was completely broken. The backflow energy appeared on the focal plane of the tightly focused FOVV beams with topological charges of $n = 1.2, m = 3.2$ in Figure 3(a₁–a₃) and $n = 1.6, m = 3.6$ in Figure 3(b₁–b₃). Comparing these two beams, we can find that there is a relationship between the topological charges of $n - m = -2$. From Figures 2 and 3, we can draw an important conclusion: that the axisymmetric backflow energy appears when the vortex topological charge n and the polarization topological charge m of a FOVV beam satisfy the condition of $n + m = 2$ or $n - m = -2$. Reviewing Figure 1(a₃,c₃), one can find that if the sum of the binary topological charges deviates from 2, or the difference of them deviates from -2 , the axisymmetric longitudinal energy on the focal plane is disrupted, and as the deviation value increases the reverse energy becomes smaller (as shown in Figure 1(a₃)), or even zero (as shown in Figure 1(c₃)).

The underlying physics of the phenomena were further explored by considering that a FOVV beam could be superposed by two vortex circularly polarized beams, which could be expressed as follows:

$$\begin{aligned} \vec{E}_i &= e^{in\phi} \left[\cos(m\phi)\hat{e}_x + \sin(m\phi)\hat{e}_y \right] \sim e^{i(n+m)\phi} (\hat{e}_x - i\hat{e}_y) + e^{i(n-m)\phi} (\hat{e}_x + i\hat{e}_y) \\ &\sim e^{i(n+m)\phi} \hat{e}_- + e^{i(n-m)\phi} \hat{e}_+. \end{aligned} \quad (3)$$

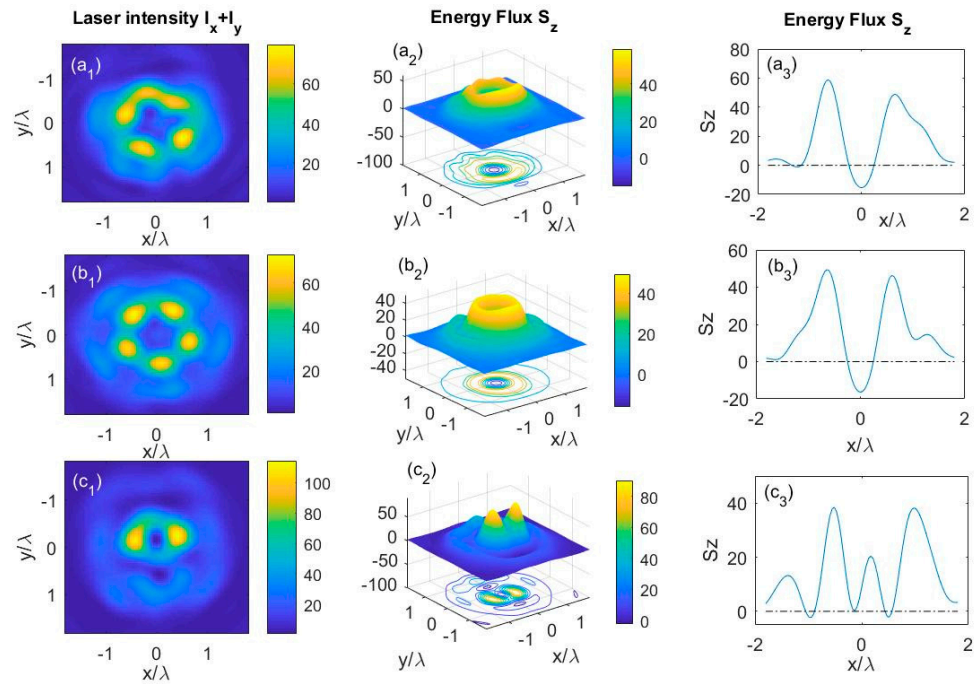


Figure 3. The intensity distributions of transverse light fields for tightly-focused beams at the focal plane, along with the corresponding longitudinal energy fluxes of vector vortex fields carrying the fractional topological charges of (a₁–a₃) $n = 1.2, m = 3.2$, (b₁–b₃) $n = 1.6, m = 3.6$, and (c₁–c₃) $n = 1.6, m = 3.1$.

The contributions of the component vortex circular polarization beams of the FOVV beams within Figures 2 and 3 to the reverse energy flow were re-examined in detail, and the results are demonstrated in Figure 4. It is evident from the solid red curves in Figure 4a–e that the axisymmetric reverse energy flow was mainly caused by the second-order vortex left circularly polarized beam, as $e^{i2\phi}\hat{e}_- = e^{i2\phi}(\hat{e}_x - i\hat{e}_y)$, and the minus second-order right circularly polarized beam, as $e^{-i2\phi}\hat{e}_+ = e^{-i2\phi}(\hat{e}_x + i\hat{e}_y)$. Regardless of the magnitude of the fractional orders of the FOVV beams, the reverse energy flow will occur near the focal region as long as the fractional topological charge satisfies $n + m = 2$ or $n - m = -2$. For the case of $n = 0$ and $m = 2$ in Equation (2), both component vortex circularly polarized beams were just $e^{i2\phi}\hat{e}_-$ and $e^{-i2\phi}\hat{e}_+$. Consequently, the negative energy of the tightly focused incident vortex-free second-order ($n = 0, m = 2$) radial polarization laser field was maximized, which provides the reason behind the observed result in Ref. [4]. From Figure 4a–c, it is obvious that the longitudinal energy on the focal plane of the tightly focused integer order vortex circularly polarized beam was axisymmetric with respect to the optical axis. However, for the vortex circularly polarized beams with non-integer order marked by the black solid or the black dotted lines in Figure 4d–f, the axial symmetry of the longitudinal energy was broken.

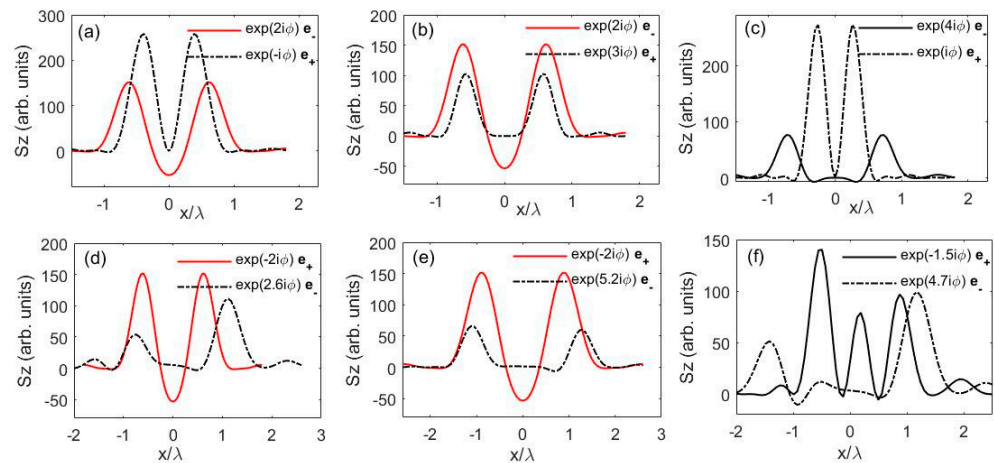


Figure 4. Contributions of the component vortex circular polarization beams to the reverse energy flow. The first row (i.e., (a–c)) corresponds to the beams in Figure 2, and the second row (i.e., (d–f)) corresponds to the beams in Figure 3.

To clarify the contributions of the component vortex circularly polarized beams in FOVV laser fields to the output axisymmetric longitudinal energy on the focal plane, we examined the focusing properties of the incident circularly polarized beams with various integer vortex orders, and the results are presented in Figure 5. Comparing Figure 5a with Figure 5d, one can find that the longitudinal energy of the vortex right circularly polarized laser fields with integer vortex order was the same as that of the vortex left circularly polarized laser fields with the corresponding opposite negative integer vortex order. Similarly, by comparing Figure 5b with Figure 5c, it is obvious that the cases of the vortex left circularly polarized laser fields with integer vortex order and the vortex right circularly polarized laser fields with the corresponding opposite negative integer vortex order were identical too. Further calculations revealed that for an arbitrary integer s the distributions of the electric vector on the cross-section of the laser beams of the pair components of $e^{\pm is\phi}\hat{e}_-$ and $e^{\mp is\phi}\hat{e}_+$ were exactly identical, so after being tightly focused the property of the energy flow near the focal region was just the same. In Figure 5a,d, there was a region in the center of the beam around the optical axis where the longitudinal energy was negligible or almost nonexistent. As the absolute value of the vortex order increased, the non-longitudinal energy region widened, resulting in energy hollow beams on the focal plane. Comparing Figure 5b with Figure 5c, it can be observed that backflow energy appeared for the vortex left circular beams as $e^{i2\phi}\hat{e}_-$, $e^{i3\phi}\hat{e}_-$, and $e^{i4\phi}\hat{e}_-$ in Figure 5b, and for the vortex right circularly polarized beams as $e^{-i2\phi}\hat{e}_+$, $e^{-i3\phi}\hat{e}_+$, and $e^{-i4\phi}\hat{e}_+$, in Figure 5c. For the circularly polarized beams of $e^{i3\phi}\hat{e}_-$, $e^{i4\phi}\hat{e}_-$ in Figure 5b, and $e^{-i3\phi}\hat{e}_+$, $e^{-i4\phi}\hat{e}_+$ in Figure 5c, there was no longitudinal energy along the optical axis. Increasing the distance from the axis, a reverse energy flow ring emerged around the optical axis on the focal plane, followed by a higher positive longitudinal energy flow ring. Comparing the cases of $e^{i3\phi}\hat{e}_-$ and $e^{i4\phi}\hat{e}_-$ in Figure 5b, one could find that as the absolute value of the vortex order increased, the non-longitudinal energy region became wider and that caused the reverse longitudinal energy rings on the focal plane to slightly shift away from the axis. If the vortex order was large enough, there was no longitudinal energy within a wider axis symmetrical region around the optical axis.

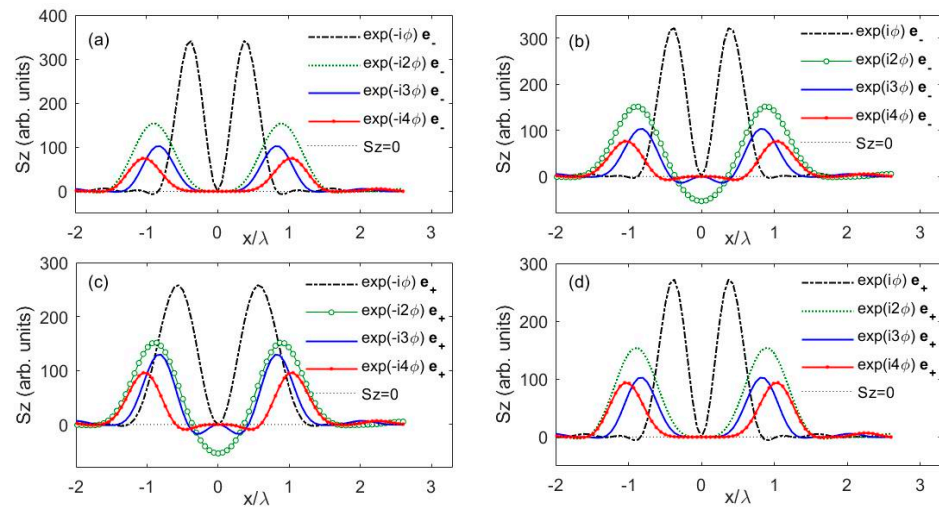


Figure 5. Output longitudinal energy flow on the focal plane of the incident integer order vortex circularly polarized beams focused by a high NA. The cases of incident left-circularly polarized beams are shown in (a,b), while (c,d) depicted the cases of incident right-circularly polarized beams.

4. Discussion

Different from the homogeneous polarized laser fields with uniform SOP, the vector vortex beams exhibited diverse SOP characteristics at different spatial positions, accompanied by spiral wavefronts and phase singularities. Because of the vector nature, the SOP will be rearranged after being focused by a high NA, which leads to the variation in the energy flow direction of the laser field, even appearing as the reverse energy flow. Based on the vortex nature, each photon of the vortex light field carried a specific amount of orbital angular momentum, which served as both an information carrier and a means of particles manipulating. Different focusing characteristics of FOVV beams are mainly caused by the transverse electric vector distributions on the cross-section of the incident laser fields. By taking a FOVV beam as a superposition of two circularly polarized vortex beams, the focusing properties could be demonstrated directly with the focusing cases of the component vortex circularly polarized beams. The tightly focusing property of the FOVV beam broadened the means of microparticle manipulation. By matching the binary topological charges of the required FOVV beams, one can anticipate and even design the energy flow distribution on the focal plane for the better manipulation of microscopic particles.

5. Conclusions

For the tightly focused FOVV beams with binary topological charges, the reverse energy flow appeared near the focal region when the fractional topological charge m and the vortex topological charge n satisfied the condition of $n + m = 2$ or $n - m = -2$. Our research reveals that the minus second-order vortex right circularly polarized beam, described by $e^{-i2\phi}\hat{e}_+$, and the second-order vortex left circularly polarized beam, described by $e^{i2\phi}\hat{e}_-$, played significant roles in generating the reverse energy flow at the focal region. This finding provides a comprehensive explanation for the observed maximum negative energy flux density of the tightly focused incident vortex-free second-order ($n = 0, m = 2$) radial polarization laser field [4]. Moreover, if the algebraic sum and the difference in the two topological charges m and n of a FOVV beam are integers, the longitudinal energy on the focal plane exhibits axis symmetry. Adjusting the appropriate values of n and m , one can obtain laser beams with a customized longitudinal energy distribution at the focal region.

Author Contributions: Conceptualization, R.C.; methodology, Y.W.; software, Y.W.; validation, Y.L. and X.H.; formal analysis, Y.W.; investigation, Y.W.; resources, Y.L.; data curation, Y.W.; writing—original draft preparation, Y.W.; writing—review and editing, Y.L. and R.C.; visualization, Y.W.; supervision, Y.L.; project administration, R.C.; funding acquisition, R.C. All authors have read and agreed to the published version of the manuscript.

Funding: This research was funded by the Zhejiang province basic public welfare research program project of China, grant number LGG21A040003, and the National Natural Science Foundation of China, grant numbers 11874323, 11574271, and 62105291.

Institutional Review Board Statement: Not applicable.

Informed Consent Statement: Not applicable.

Data Availability Statement: The data presented in this study are available on request from the corresponding author.

Conflicts of Interest: The authors declare no conflict of interest.

References

1. Youngworth, K.S.; Brown, T.G. Focusing of High Numerical Aperture Cylindrical Vector Beams. *Opt. Express* **2000**, *7*, 77–87. [[CrossRef](#)] [[PubMed](#)]
2. Novitsky, A.V.; Novitsky, D.V. Negative propagation of vector Bessel beams. *J. Opt. Soc. Am. A* **2007**, *24*, 2844–2848. [[CrossRef](#)] [[PubMed](#)]
3. Kotlyar, V.V.; Kovalev, A.A.; Nalimov, A.G. Energy density and energy flux in the focus of an optical vortex: Reverse flux of light energy. *Opt. Lett.* **2018**, *43*, 2921–2924. [[CrossRef](#)] [[PubMed](#)]
4. Khonina, S.N.; Ustinov, A.V.; Degtyarev, S.A. Inverse energy flux of focused radially polarized optical beams. *Phys. Rev. A* **2018**, *98*, 043823. [[CrossRef](#)]
5. Kotlyar, V.V.; Stafeev, S.S.; Nalimov, A.G. Energy backflow in the focus of a light beam with phase or polarization singularity. *Phys. Rev. A* **2019**, *99*, 033840. [[CrossRef](#)]
6. Kotlyar, V.V.; Stafeev, S.S.; Kovalev, A.A. Reverse and toroidal flux of light fields with both phase and polarization higher-order singularities in the sharp focus area. *Opt. Express* **2019**, *27*, 16689–16702. [[CrossRef](#)]
7. Li, H.; Wang, C.; Tang, M.; Li, X. Controlled negative energy flow in the focus of a radial polarized optical beam. *Opt. Express* **2020**, *28*, 18607–18615. [[CrossRef](#)]
8. Yu, C.; He, Z.; Huang, C.; Chen, F.; Zeng, J.; Li, Y.; Zhang, Y.; Pu, J.; Lin, H. Tight focusing properties of ring pearcey beams with a cross phase. *Photonics* **2022**, *9*, 964. [[CrossRef](#)]
9. Yuan, G.H.; Rogers, E.T.F.; Zheludev, N.I. “Plasmonics” in free space: Observation of giant wavevectors, vortices and energy backflow in superoscillatory optical fields. *Light Sci. Appl.* **2017**, *6*, 17036. [[CrossRef](#)]
10. Kotlyar, V.V.; Nalimov, A.G. Focusing a vortex laser beam and converting linear to circular polarization. *Laser Phys.* **2021**, *31*, 116205. [[CrossRef](#)]
11. McLeod, R.R.; Daiber, A.J.; McDonald, M.E.; Robertson, T.L.; Slagle, T.; Sochava, S.L.; Hesselink, L. Microholographic multilayer optical disk data storage. *Appl. Opt.* **2005**, *44*, 3197–3207. [[CrossRef](#)] [[PubMed](#)]
12. Xian, M.; Xu, Y.; Ouyang, X.; Cao, Y.; Lan, S.; Li, X. Segmented cylindrical vector beams for massively-encoded optical data storage. *Sci. Bull.* **2020**, *65*, 2072–2079. [[CrossRef](#)] [[PubMed](#)]
13. Wang, J. Advances in communications using optical vortices. *Photonics Res.* **2016**, *4*, B14–B28. [[CrossRef](#)]
14. Willner, A.E.; Huang, H.; Yan, Y.; Ren, Y.; Ahmed, N.; Xie, G.; Bao, C.; Li, L.; Cao, Y.; Zhao, Z.; et al. Optical communications using orbital angular momentum beams. *Adv. Opt. Photonics* **2015**, *7*, 66–106. [[CrossRef](#)]
15. Cui, X.; Yin, X.; Chang, H.; Liao, H.; Chen, X.; Xin, X.; Wang, Y. Experimental study of machine-learning-based orbital angular momentum shift keying decoders in optical underwater channels. *Opt. Commun.* **2019**, *452*, 116–123. [[CrossRef](#)]
16. Ouyang, X.; Xu, Y.; Xian, M.; Feng, Z.; Zhu, L.; Cao, Y.; Lan, S.; Guan, B.-O.; Qiu, C.-W.; Gu, M.; et al. Synthetic helical dichroism for six-dimensional optical orbital angular momentum multiplexing. *Nat. Photonics* **2021**, *15*, 901–907. [[CrossRef](#)]
17. Planchon, T.A.; Gao, L.; Milkie, D.; Davidson, M.W.; Galbraith, J.A.; Galbraith, C.G.; Betzig, E. Rapid three-dimensional isotropic imaging of living cells using Bessel beam plane illumination. *Nat. Methods* **2011**, *8*, 417–423. [[CrossRef](#)]
18. Wang, Y.; Wang, Y.; Guo, Z. OAM radar based fast super-resolution imaging. *Measurement* **2022**, *189*, 110600. [[CrossRef](#)]
19. Padgett, M.; Bowman, R. Tweezers with a twist. *Nat. Photonics* **2011**, *5*, 343–348. [[CrossRef](#)]
20. Wang, X.-L.; Ding, J.; Ni, W.-J.; Guo, C.-S.; Wang, H.-T. Generation of arbitrary vector beams with a spatial light modulator and a common path interferometric arrangement. *Opt. Lett.* **2007**, *32*, 3549–3551. [[CrossRef](#)]

21. Richards, B.; Wolf, E. Electromagnetic diffraction in optical systems. II. Structure of the image field in an aplanatic system. *Proc. R. Soc. Lond. Ser. A Math. Phys. Sci.* **1959**, *253*, 358–379.
22. Pan, D.; Chew, K.-H.; Wu, Y.; Chen, R.-P. Conversions of linear-circular polarizations and spin-orbital angular momentums in a focused vector vortex beam with fractional topological charges. *Opt. Int. J. Light Electron Opt.* **2022**, *252*, 168473. [[CrossRef](#)]

Disclaimer/Publisher’s Note: The statements, opinions and data contained in all publications are solely those of the individual author(s) and contributor(s) and not of MDPI and/or the editor(s). MDPI and/or the editor(s) disclaim responsibility for any injury to people or property resulting from any ideas, methods, instructions or products referred to in the content.